Notes on Numerical Fluid Mechanics and Multidisciplinary Design 142

Andreas Dillmann
Gerd Heller
Ewald Krämer
Claus Wagner
Cameron Tropea
Suad Jakirlić *Editors*

New Results in Numerical and Experimental Fluid Mechanics XII

Contributions to the 21st STAB/DGLR Symposium, Darmstadt, Germany, 2018

Springer

Notes on Numerical Fluid Mechanics and Multidisciplinary Design

Volume 142

Founding Editor

Ernst Heinrich Hirschel, Zorneding, Germany

Series Editors

Wolfgang Schröder, Aerodynamisches Institut, RWTH Aachen, Aachen, Germany
Bendiks Jan Boersma, Delft University of Technology, Delft, The Netherlands
Kozo Fujii, Institute of Space & Astronautical Science (ISAS), Sagamihara, Kanagawa, Japan
Werner Haase, Hohenbrunn, Germany
Michael A. Leschziner, Department of Aeronautics, Imperial College, London, UK
Jacques Periaux, Paris, France
Sergio Pirozzoli, Dept. Mechanical and Aerospace Eng., University of Rome 'La Sapienza', Roma, Italy
Arthur Rizzi, Department of Aeronautics, KTH Royal Institute of Technology, Stockholm, Sweden
Bernard Roux, Ecole Supérieure d'Ingénieurs de Marseille, Marseille CX 20, France
Yurii I. Shokin, Siberian Branch of the Russian Academy of Sciences, Novosibirsk, Russia

Notes on Numerical Fluid Mechanics and Multidisciplinary Design publishes state-of-art methods (including high performance methods) for numerical fluid mechanics, numerical simulation and multidisciplinary design optimization. The series includes proceedings of specialized conferences and workshops, as well as relevant project reports and monographs.

More information about this series at http://www.springer.com/series/4629

Andreas Dillmann · Gerd Heller ·
Ewald Krämer · Claus Wagner ·
Cameron Tropea · Suad Jakirlić
Editors

New Results in Numerical and Experimental Fluid Mechanics XII

Contributions to the 21st STAB/DGLR Symposium, Darmstadt, Germany, 2018

Springer

Editors
Andreas Dillmann
Deutsches Zentrum für Luft- und Raumfahrt
Institut für Aerodynamik
und Strömungstechnik
Göttingen, Niedersachsen, Germany

Ewald Krämer
Institut für Aerodynamik und Gasdynamik
Universität Stuttgart
Stuttgart, Baden-Württemberg, Germany

Cameron Tropea
Fachgebiet Strömungslehre
und Aerodynamik
Technische Universität Darmstadt
Darmstadt, Hessen, Germany

Gerd Heller
Airbus Operations GmbH
Bremen, Bremen, Germany

Claus Wagner
Deutsches Zentrum für Luft- und Raumfahrt
Institut für Aerodynamik
und Strömungstechnik
Göttingen, Niedersachsen, Germany

Suad Jakirlić
Fachgebiet Strömungslehre
und Aerodynamik
Technische Universität Darmstadt
Darmstadt, Hessen, Germany

ISSN 1612-2909 ISSN 1860-0824 (electronic)
Notes on Numerical Fluid Mechanics and Multidisciplinary Design
ISBN 978-3-030-25252-6 ISBN 978-3-030-25253-3 (eBook)
https://doi.org/10.1007/978-3-030-25253-3

© Springer Nature Switzerland AG 2020
This work is subject to copyright. All rights are reserved by the Publisher, whether the whole or part of the material is concerned, specifically the rights of translation, reprinting, reuse of illustrations, recitation, broadcasting, reproduction on microfilms or in any other physical way, and transmission or information storage and retrieval, electronic adaptation, computer software, or by similar or dissimilar methodology now known or hereafter developed.
The use of general descriptive names, registered names, trademarks, service marks, etc. in this publication does not imply, even in the absence of a specific statement, that such names are exempt from the relevant protective laws and regulations and therefore free for general use.
The publisher, the authors and the editors are safe to assume that the advice and information in this book are believed to be true and accurate at the date of publication. Neither the publisher nor the authors or the editors give a warranty, expressed or implied, with respect to the material contained herein or for any errors or omissions that may have been made. The publisher remains neutral with regard to jurisdictional claims in published maps and institutional affiliations.

This Springer imprint is published by the registered company Springer Nature Switzerland AG
The registered company address is: Gewerbestrasse 11, 6330 Cham, Switzerland

Foreword

This volume contains the papers presented at the 21st STAB/DGLR Symposium held in Darmstadt, Germany (November 6–7, 2018) organized by the Institute for Fluid Mechanics and Aerodynamics at the Technische Universität Darmstadt. STAB is the German Aerospace Aerodynamics Association (Deutsche Strömungsmechanische Arbeitsgemeinschaft) founded towards the end of the 1970s, and DGLR is the German Society for Aeronautics and Astronautics (Deutsche Gesellschaft für Luft- und Raumfahrt - Lilienthal Oberth e.V.).

The mission of STAB is to foster aerodynamics research and its appreciation in Germany. This is accomplished by creating forums for scientific discussions and by disseminating most recent research results, thereby enhancing scientific progress and avoiding unnecessary duplication in research work.

STAB brings together German scientists and engineers from universities, research establishments and industry. They present research and project work in numerical and experimental fluid mechanics as well as aerodynamics for diverse fields, such as aeronautics, space, ground transportation, wind turbines and other applications. This format also offers an excellent opportunity for exchange about numerous common research activities sponsored by different funding agencies.

Since 1986 the symposium takes place every two years at different locations in Germany, all having an affinity to fluid mechanics and aerodynamics.

In addition STAB Workshops are held regularly at DLR (Deutsches Zentrum für Luft- und Raumfahrt) in Göttingen in the intermediate years.

Both, STAB symposia and workshops provide excellent forums where new research activities can be presented, often resulting in new jointly organized research and technology projects.

In this volume symposium contributions are published for the twelfth time, following a thorough peer review.

The review board, comprising also the programme committee, consisted of P. Bahavar (Göttingen), C. Bauer (Göttingen), J. Bell (Göttingen), T. Berkefeld (Göttingen), I. Bolgar (Neubiberg), A. Botelho e Souza (Braunschweig), M. Braune (Göttingen), J. Breitenbach (Darmstadt), C. Breitsamter (München), C. Brückner (Göttingen), A. Buhr (Göttingen), O. Burghardt (Kaiserslautern), M. Burnazzi

(Göttingen), M. Costantini (Göttingen), A. Dannhauer (Göttingen), J. Delfs (Braunschweig), R. du Puits (Ilmenau), K. Ehrenfried (Göttingen), R. Ewert (Braunschweig), B. Faßmann (Braunschweig), M. Fehrs (Göttingen), U. Fey (Göttingen), H. Foysi (Siegen), A. Gardner (Göttingen), D. Gatti (Karlsruhe), N. Gauger (Kaiserslautern), R. Geisler (Göttingen), C. Grabe (Göttingen), A. Guissart (Darmstadt), V. Hannemann (Göttingen), F. Heckmeier (München), M. Hehner (Karlsruhe), A. Heider (Göttingen), S. Hein (Göttingen), S. Helm (Göttingen), A. Henning (Göttingen), S. Herbst (Neubiberg), N. Herzog (Taufkirchen), S. Herzog (Göttingen), S. Hitzel (Manching), A. Hövelmann (Manching), A. Hübner (Braunschweig), D. Iglesias (Gilching), C. Ilic (Braunschweig), S. Jakirlić (Darmstadt), C. Jessing (Stuttgart), C. Kästner (Ilmenau), K. Kaufmann (Göttingen), A. Kellersmann (Braunschweig), M. Keßler (Stuttgart), T. Kilian (Braunschweig), J. Kissing (Darmstadt), D. Klatt (Saint-Louis), C. Klein (Göttingen), J. Klinner (Köln), M. Kloker (Stuttgart), T. Knopp (Göttingen), R. Konrath (Göttingen), M. Konstantinov (Göttingen), M. Kotsonis (Delft), U. Krause (Bremen), A. Krumbein (Göttingen), B. Krumbein (Darmstadt), A. Kümmel (München), P. Kunze (Braunschweig), P. Lange (Göttingen), R. Lechner (Otterfing), A. Lösch (Ilmenau), T. Lutz (Stuttgart), R. Maduta (Darmstadt), J. Martinez Schramm (Göttingen), E. Mäteling (Aachen), A. Merle (Braunschweig), B. Michels (Braunschweig), A. Mielke (Saint-Louis), M. Mommert (Göttingen), M. Müller (Göttingen), M. M. Müller (Göttingen), J. Nitzsche (Göttingen), E. Öngüner (Göttingen), J. Pflüger (München), S. Pfnür (München), P. Pölzlbauer (München), A. Probst (Göttingen), D. Puckert (Stuttgart), D. Ramaswamy (Aachen), M. Reder (Karlsruhe), A. Reeh (Taufkirchen), L. Reimer (Braunschweig), M. Rein (Göttingen), K. Richter (Göttingen), S. Risius (Göttingen), U. Rist (Stuttgart), M. Ritter (Göttingen), M. Rütten (Göttingen), S. Scharnowski (Neubiberg), J. B. Schmidt (Darmstadt), O. Schmidt (San Diego), A. Schreyer (Aachen), A. Schröder (Göttingen), E. Schülein (Göttingen), T. Schütz (München), T. Schwarz (Braunschweig), B. Selent (Stuttgart), J. Serpieri (Delft), L. Siegel (Göttingen), C. Stanger (Stuttgart), A. Stroh (Karlsruhe), M. Stuhlpfarrer (München), G. Subbian, (Braunschweig), A. Suryadi (Braunschweig), E. Tangermann (Neubiberg), J. Ullah (Stuttgart), N. van Hinsberg (Göttingen), M. Vieweg (Köln), C. Voß (Göttingen), A. Waldmann (Stuttgart), K. Weinman (Göttingen), M. Werner (Göttingen), A. Westhoff (Göttingen), T. Wetzel (Göttingen), F. Wienke (Göttingen), H. Wilhelmi (Göttingen), G. Wilke (Braunschweig), A. Winkler (Manching), M. Winter (München), Y. Wu (Stuttgart), S. Yadala (Poitiers), Y. Zhang (Darmstadt).

Nevertheless, the authors sign responsible for the contents of their contributions.

The editors are grateful to Prof. Dr. W. Schröder as the General Editor of the "Notes on Numerical Fluid Mechanics and Multidisciplinary Design" series and to the Springer publishing house for the opportunity to publish the results of the symposium.

February 2019

A. Dillmann
G. Heller
E. Krämer
C. Wagner
C. Tropea
S. Jakirlić

Contents

High-Agility Configuration

Rotorcraft Aerodynamics

Technical Flows

Aeroelasticity and Structural Dynamics

Biofluidmechanics

Airplane Aerodynamics/Propulsion Integration

Implementation of a Method to Determine Aerodynamic Propeller-Wing Interaction

Nikolai Herzog(✉) and Andreas Reeh(✉)

Siemens AG, Corporate Technology, Munich, Germany
{nikolai.herzog,andreas.reeh}@siemens.com

Abstract. The scalability and lightweight design of electric motors within (hybrid-) electric propulsion systems facilitates the distribution of propulsion. The aerodynamic interaction of a swirling propeller slipstream and a lifting surface can be beneficial regarding a vehicle's propulsive efficiency. This report presents the implementation of a numerical method of low computational effort based on Blade Element Momentum Theory combined with a Vortex Lattice Method using a simple slipstream model. Goal of the method is to determine basic effects and trends of such aerodynamic interaction effects for conducting design studies regarding principle parameters of propeller-wing tractor configurations. The implementation is depicted and a verification is given with experimental results from literature.

Keywords: Propeller-Wing · Aerodynamic Interaction · Blade Element Momentum Theory · Vortex Lattice Method

1 Introduction

Aerodynamic effects of distributed propulsion play a key role in today's research concerning next generation aircraft designs. Especially the positioning of propellers within the flow field of a wing leads to an aerodynamic interaction. For the preliminary design this topic has been investigated recently in [1,2] and [3]. In order to approach this interaction a simple method using Blade Element Momentum Theory (BEMT) and a Vortex Lattice Method (VLM) is implemented based on [4]. The propeller calculation uses the induced velocities of a wing's three-dimensional (3D) flow field on the propeller disc and vice versa the wing calculation considers propeller-induced velocities. It represents a preliminary design approach to model aerodynamic interaction effects regarding principle geometry parameters. Thus, by approaching the complex and unsteady flow with a stationary and rather simple approach, this method is suited for parameter studies. The aerodynamic interaction of an exemplary propeller-wing configuration has been investigated experimentally in [5,6] and [7] using a wind-tunnel model, whose results are used here for a verification of the implemented method. Figure 1 presents qualitatively the interaction problem by showing two-dimensional (2D) streamlines of isolated and combined flow fields.

© Springer Nature Switzerland AG 2020
A. Dillmann et al. (Eds.): DGLR 2018, NNFM 142, pp. 3–13, 2020.
https://doi.org/10.1007/978-3-030-25253-3_1

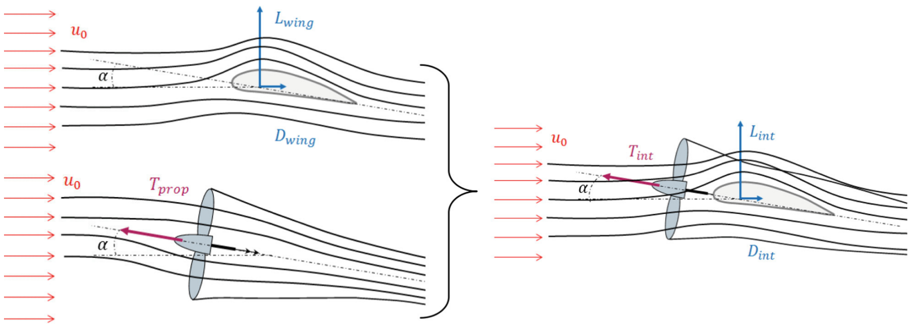

Fig. 1. Qualitative visualization of the aerodynamic interaction of the flow fields.

2 Physical Modeling

The propeller flow is modeled using BEMT extended with azimuthal discretization to consider arbitrary 3D inflow on the propeller disc using a quasi-steady sector approach. This provides the forces and moments of the propeller and the flow field input for a simple inviscid and non-deflected slipstream model. Latter is used to transfer the propeller induced velocities of each radial and azimuthal propeller disc position onto the collocation points of the VLM with a velocity development which is dependent on local slipstream contraction. Local induced velocity and Angle of Attack (AoA) at the panels are taken into account to complement the boundary condition of no perpendicular flow. On each panel the element-wise lift and drag force components are evaluated. This procedure already provides good results for the verification case approached here and is named Single Interaction Mode (SIM) as mentioned in [4]. A Full Interaction Mode (FIM) is also implemented here, but with the use of a convergence loop for the propeller induced velocity field at the propeller disc, as shown in the flow chart of Fig. 2.

2.1 Blade Element Momentum Theory

The BEMT is implemented using the equations from [8] and its governing set of non-linear equations. The equations for each blade element on non-dimensional radial position $\xi = r/R$ are extended for azimuthal angle θ reading

$$\frac{a}{1+a} = \frac{\sigma c_y}{4F\,\sin^2\phi} \tag{1}$$

$$\frac{a'}{1-a'} = \frac{\sigma c_x}{4F\,\cos\phi\,\sin\phi} \tag{2}$$

$$\phi = \arctan\frac{u_0\,\cos\alpha_p\,\cos\beta_p\,(1+a)}{(u_0\,(\sin\alpha_p\,\cos\beta_p\,\sin\theta\,+\,\sin\beta_p\cos\theta)\,+\,\Omega r)\,\,(1-a')} \tag{3}$$

where a, a' and $\phi = \beta - \alpha_i$ represent the axial interference factor, the tangential interference factor and the flow angle as a difference of the blade sectional twist angle β and induced angle of attack α_i. These three unknowns are determined for each non-dimensional radial position ξ and azimuthal angle θ of the propeller disc considering the local angle of attack α_p and local sideslip angle β_p. B represents the number of blades, c the sectional chord length, $\sigma = \frac{Bc}{2\pi\xi R}$ the sectional solidity ratio, u_0 the inflow velocity and Ω the angular velocity of the propeller. The section force coefficients $c_x = c_L \sin\phi + c_D \cos\phi$ and $c_y = c_L \cos\phi - c_D \sin\phi$ are obtained using 2D airfoil polar data. The losses induced by the flow around the blade tips are modeled using the Prandtl tip loss factor F. The non-linear equations are solved iteratively for each radial and azimuthal position to determine the respective incremental values for thrust and torque and induced axial and tangential velocity components. A spatial discretization of 16 radial and 12 azimuthal elements is used. Unsteady in-plane forces and moments varying per revolution are not taken into account within this approach.

2.2 Slipstream Model

The flow passing through the propeller disc is assumed to contract according to a slipstream contraction factor given in [10] with the assumption of kinematic energy conservation. The contraction is here extended for azimuthal dependency and given by

$$\frac{r_s}{r} = \sqrt{\frac{1+a}{1+a\left(1+\frac{x_s}{\sqrt{r^2+x_s^2}}\right)}}, \tag{4}$$

where r_s/r denotes the radial contraction at the axial distance x_s within the slipstream. The axial and tangential velocities $u_{s,ax}$ and $u_{s,t}$ at this distance behind the propeller-disk read

$$u_{s,ax} = \left(\frac{r}{r_s}\right)^2 u_{p,ax} \; and \; u_{s,t} = \frac{r}{r_s} u_{p,t}, \tag{5}$$

where $u_{p,ax}$ and $u_{p,t}$ denote the axial and tangential velocity components at the propeller disc obtained from the BEMT.

2.3 Vortex Lattice Method

The VLM is implemented according to [9] and the adaption for the propeller influence is implemented as described in [4]. The trailing vortices are aligned with the wing's chord direction. If a panel is located within the propeller streamtube, the velocity vector at this collocation point considers the propeller-induced slipstream velocity reading $\mathbf{u}_i = \mathbf{u}_0 + \mathbf{u}_{s,i}$. The velocities induced by all horseshoe vortices onto all collocation points are formulated mathematically with the Biot-Savart law. Here the equation for discrete, straight vortex segments of finite length is applied, given by

$$\mathbf{u} = \frac{\Gamma}{4\pi} \frac{\mathbf{r}_1 \times \mathbf{r}_2}{|\mathbf{r}_1 \times \mathbf{r}_2|^2} \left[\mathbf{r}_0 \left(\frac{\mathbf{r}_1}{r_1} - \frac{\mathbf{r}_2}{r_2}\right)\right] \tag{6}$$

where Γ is the circulation of the vortex segment between $\mathbf{r}_1$ and $\mathbf{r}_2$ and $\mathbf{u}$ the induced velocity at $\mathbf{r}_0$. This law is applied for all bound and trailing vortices to set up equations for the normal components of the induced velocities of all horseshoe vortices onto all panel collocation points.

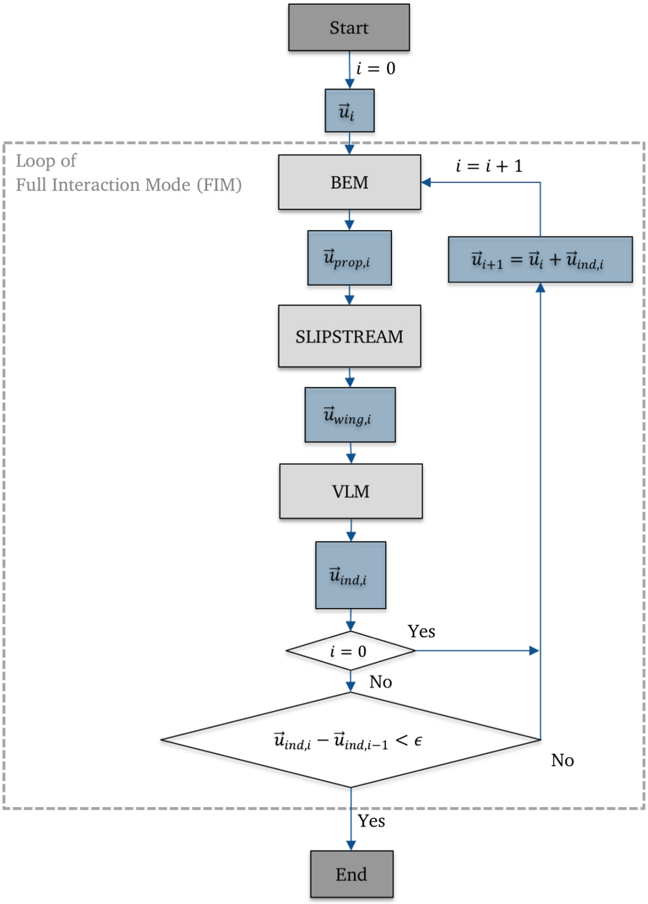

Fig. 2. Flow chart for the BEMT-VLM coupling within the interaction loop.

The boundary condition of zero normal flow at these points leads to the set of linear algebraic equations for the unknown circulation strengths reading $a_{ij}\Gamma_j = -\mathbf{u}_i \cdot \mathbf{n}_i$, where a_{ij} represents the influence coefficient of the j-th circulation strength onto the i-th panel by $a_{ij} = \mathbf{u}_{ind,ij} \cdot \mathbf{n}_i$. The boundary condition on the right side denoted by $-\mathbf{u}_i \cdot \mathbf{n}_i$ is the negative value of local velocity normal to the i-th panel surface. As the circulation values at all panels are known, the lift of the i-th panel and per unit span is obtained by $\mathbf{l}_i = \rho \mathbf{u}_i \mathbf{\Gamma}_i$. Here especially within the propeller slipstream the direction of the local inflow vector is considered tilting the lift vector compared to a panel which is not located in the slipstream. In a next step, the induced angle of attack $\alpha_{ind,i}$ and thus resulting induced drag components d_i are evaluated for all panels. The induced velocities at the collocation points $w_{ind,i}$ are calculated with influence coefficients b_{ij}, taking exclusively the trailing vortices into account. These read $b_{ij} = \mathbf{u}^*_{ind,ij} \cdot \mathbf{n}_i$ with $\mathbf{u}^*_{ind,ij}$ being the induced velocity vectors only by the trailing vortices. With the original determined circulation strengths Γ_j, the induced velocities are obtained reading $w_{ind,i} = b_{ij}\Gamma_j$. A panel's induced angle of attack then reads $\alpha_{ind,i} = arctan(w_{ind,i}/u_i)$. Finally the section-wise drag components by wing thickness and surface friction are obtained via XFoil and added to the induced drag components.

3 Results

In order to verify the implemented BEMT-VLM method the configuration described in [5] is modeled and aerodynamic force coefficients are compared to the experimental results. At first the aerodynamics of the isolated propeller and isolated wing are verified. It follows the calculation of the full propeller-wing configuration at one exemplary operating point to evaluate both induced velocity components and sectional lift and drag characteristics. Finally the configuration's force coefficients are calculated over an AoA-range with propeller-off and four different thrust settings and inflow velocity values. The model dimensions and airfoils used are given in [7].

3.1 Verification of BEMT and VLM

The calculated isolated propeller efficiency $\eta = J\frac{C_T}{C_P}$ is shown in Fig. 3 over the advance ratio $J = \frac{u}{nD}$, where C_T is the thrust coefficient, C_P the power coefficient, u the inflow velocity, n the rotations per second and D the propeller diameter. Two different pitch settings $\beta_{0.75R} = 8°$ and $\beta_{0.75R} = 20°$ are applied. The used thrust coefficients C^*_T throughout the experimental report are based on dynamic slipstream pressure reading

$$C^*_T = \frac{T}{q^*_0 S_{prop}} \; with \; q^*_0 = \frac{\rho}{2}u^2 + \frac{T}{S_{prop}}, \tag{7}$$

where T is the propeller thrust and S_{prop} its disc area. It is used to avoid infinite force coefficients at zero wind-tunnel velocity. The main geometry parameters of the propeller blades are given in terms of twist, chord and airfoil thickness distribution. The given CLARK-Y airfoil for the propeller with a thickness of 11.7% is located only at $0.5R$. Since no further geometry information is available, the CLARK-Y geometry is assumed to be representative for all other radial sections within this approach. Airfoil data is generated using XFoil and sectional Reynolds number.

Furthermore propeller nacelle influence is not considered and propeller radial elements are accounted starting at $0.2R$. These are all possible reasons for large

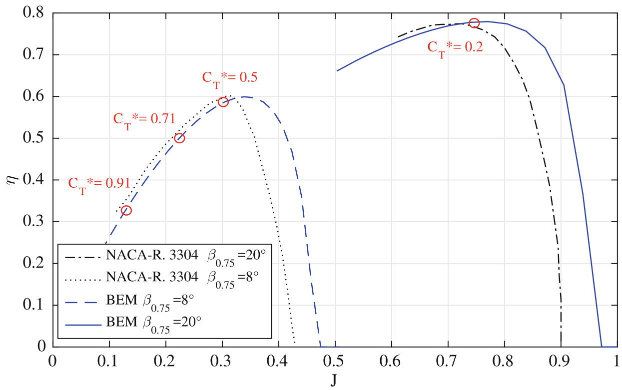

Fig. 3. Calculated propeller efficiency compared with experimental data.

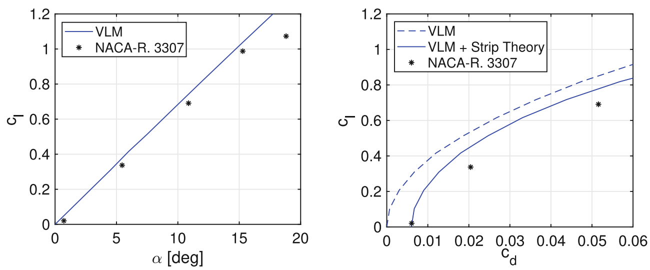

Fig. 4. Lift coefficient over *AoA* and drag polar for inviscid and viscid approach.

deviations to experimental results but are accepted here since emphasis is laid on evaluation of principle effects of the propeller-wing interaction. However the efficiency for the propeller at the points of interest is calculated with reasonable accuracy, as marked in Fig. 3. Within a next step the VLM results for the clean wing of the configuration are compared to the experimental polar in Fig. 4. NACA0015 polar data for including strip-wise the airfoil pressure and friction drag is generated also with XFoil under sectional Reynolds number. The α-c_L-curve shows good accuracy and the linear behavior, due to the used VLM implementation. Next to the experimental drag polar, the inviscid and viscid results are shown on the right side of Fig. 4. The calculated drag polar shows good agreement for the zero *AoA* case, but underestimates the experimental drag values with increasing lift coefficient.

3.2 Verification of the Combined Method

In order to verify the correct implementation of propeller slipstream velocity components onto the VLM panels, the propeller-wing configuration is calculated at an exemplary operation point at medium thrust coefficient of $C_T^* = 0.5$ and $AoA = 6°$.

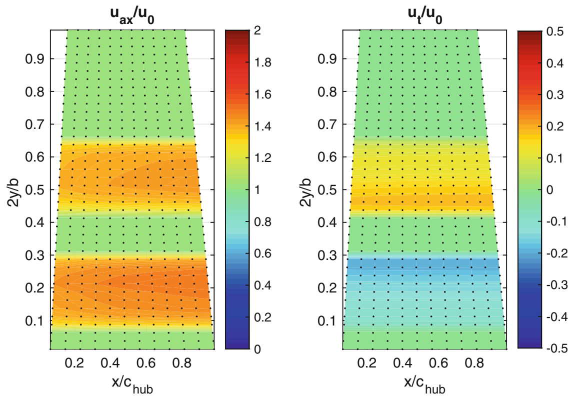

Fig. 5. Top-view showing non-dimensional slipstream velocity components.

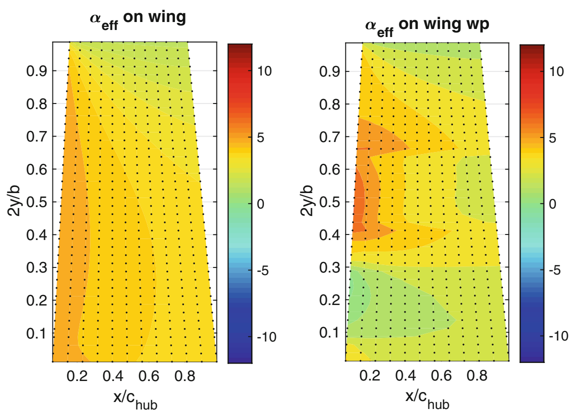

Fig. 6. Prop-off vs. Prop-on case comparing effective *AoA* at the VLM panels.

The top-view of the semi-wing is shown in Fig. 5 with the propeller located left to it and rotating outboard-up direction. The non-dimensional axial and tangential velocity components obtained from the propeller calculation and resulting from the slipstream model can be seen at the respective VLM collocation points behind the propeller. The inner blade, being here the advancing blade, shows slightly larger axial velocity values than on the retreating blade side (left). Considering the sign of the tangential induced velocity (right), the outboard-up rotation of the stream-tube is verified. Moreover for this operation condition the local effective *AoA* at the VLM panels is shown in Fig. 6 for the propeller-off case (left) and with the influence of the propeller slipstream flow (right). Keeping this in mind Fig. 7 (left) shows the sectional values for lift and drag coefficient, compared to the isolated wing characteristics for the described condition. The coefficient values are related to free-stream velocity. Figure 7 (right) shows a

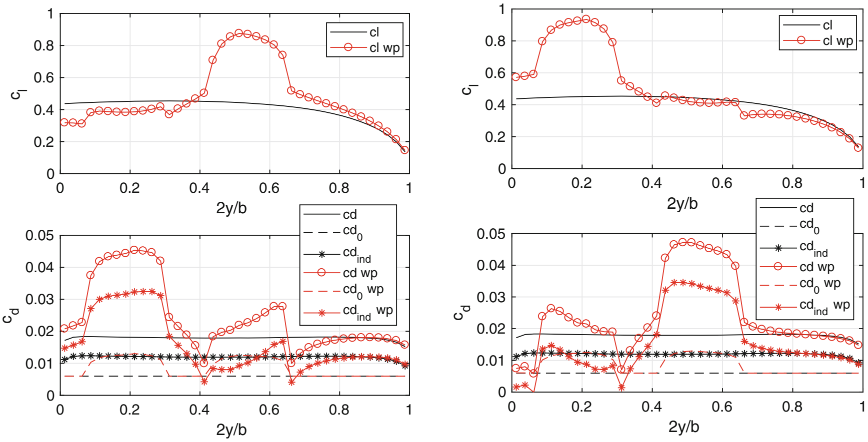

Fig. 7. Outboard-up (left) vs. inboard-up rotation at $C_T^* = 0.5$ and $AoA = 6°$.

result for everything maintained but inboard-up rotation of the propeller, as a comparison. Within the upper plots a clear increase of sectional lift coefficient can be detected behind the upward rotating blade side combined with an increase in local induced drag on the downward rotating blade side. The lower plots compare the sectional drag coefficients also including the propeller effect against the propeller-off case. Additionally the internal values for sectional parasitic and sectional induced drag contributing to the total sectional drag coefficients are shown. The effect of increased parasitic drag behind the propeller can be seen. The induced drag coefficient may be related to the local tilt of a panel's lift vector resulting from the effective AoA at each panel. The shown results are achieved with a converged interaction loop of induced propeller disc velocities (FIM) but differ negligible from the SIM results.

3.3 Verification of the Propeller-Wing Configuration

The considered experimental results provide vertical and horizontal force coefficients of the full configuration at different AoA over a velocity range with simultaneously reducing the propeller loading. The operating conditions for each AoA-sweep are listed in Table 1.

Table 1. Wind-tunnel velocity and isolated propeller thrust settings.

$\mathbf{u_0}$[m/s]	**J**[−]	$\beta_{0.75}$[°]	$\mathbf{C_T^*}$[−]	$\mathbf{C_T}$[−]	**DL**[N/m²]	**RPM**
25.00	-	-	-	-	-	-
22.31	0.74	20	0.20	0.0570	78.08	2936
17.65	0.30	8	0.50	0.0359	192.03	5811
13.47	0.22	8	0.71	0.0499	271.52	5887
7.49	0.13	8	0.91	0.0663	348.20	5811

In order to compare force coefficients c_Y^* and c_X^* of the tractor configuration, the propeller reaction forces also have to be included. The convention given in [5] is used reading

$$c_Y^* = \frac{L + T \sin\alpha}{q_0^* S_{wing}} \; and \; c_X^* = \frac{D - T\cos\alpha}{q_0^* S_{wing}}, \tag{8}$$

where L, D are the calculated lift and drag values for the blown wing, S_{wing} the projected wing surface and T the calculated propeller thrust. The different propeller thrust values are achieved by iterating the propeller RPM as it was made within the experimental campaign. For all wind-tunnel velocity and thrust value combinations thus an equal dynamic slipstream pressure of $q_0^* = 383\,\text{N/m}^2$ is maintained. The force coefficients for the configuration are shown in Fig. 8.

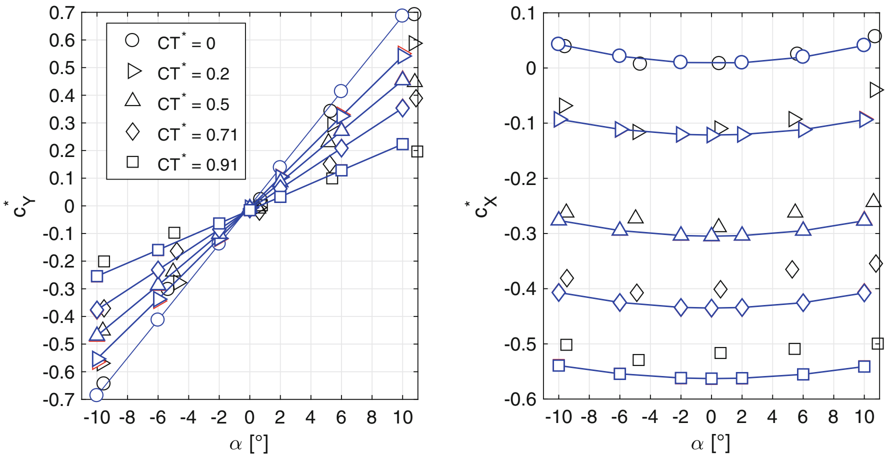

Fig. 8. Computational force coefficients c_X^* and c_Y^* (connected symbols) are compared to experimental results (symbols only) over inflow angle.

The FIM results (blue, connected symbols) are shown and match to the SIM results (red symbols), where these are not visible. In general there are slightly different results by FIM and SIM. The lightest propeller loading result, representing a fast cruise state, shows the largest difference of a 1.6% lower c_Y^* at $AoA = 10°$ for the FIM compared to SIM. The experimental c_Y^* results (black, unconnected symbols) are met with reasonable accuracy but in general the trend is captured quite well. The horizontal force coefficients c_X^* have decreasing agreement to the experimental values with increasing thrust coefficient. The drag increase with increasing AoA is captured for all disc loading conditions. Finally the vertical and horizontal force coefficients are compared at 6° and −6° for the described state with $C_T^* = 0.5$. For the computational results these cases represent outboard-up and inboard-up rotation direction, since the wing airfoil is symmetric. The quotient c_Y^*/c_X^* shows an increase of 6% for the inboard-up rotation compared to outboard-up direction, which depicts an example of a trend analysis for such a propeller-wing configuration.

4 Conclusion

A preliminary design tool for the aerodynamic interaction of propeller-wing tractor configurations has been implemented and computational results of a reference configuration have been presented. The approach is based on Blade Element Momentum Theory (BEMT) combined with a Vortex Lattice Method (VLM) using a simple slipstream model and enables to capture quasi-steady interaction of the flow fields. The BEMT and VLM match well with the available experimental data for the isolated components under the operation points of interest. The internal results of the combined method show its capability to capture principle interaction effects. The calculation of force coefficients of a wind-tunnel model from literature show good agreement regarding the trend of the vertical force coefficients. Although both a Single Interaction Mode and a Full Interaction Mode using a convergence loop for the induced velocity field on the propeller disc have been implemented, only the lightly loaded propeller case shows a deviation in the order of 1–2% for the vertical force component. In a next step further geometries have to be calculated and a comparison to finite-volume based methods shall be made for further verification. Although the interaction of a propeller and a wing constitutes a highly complex interaction problem, this method of low computational cost can be used in optimization loops to match propeller and wing preliminary designs. The method enables sensitivity analysis to different propeller principle designs with e.g. blade counts, tip speeds and in general the governing individual slipstream flow field.

References

1. Ferraro, G., Kipouros, T., Savill, M., Rampurawala, A., Agostinelli, C.: Propeller-Wing Interaction Prediction for Early Design. AIAA SciTech, Maryland (2014)
2. Patterson, M.D.: Conceptual design of high-lift propeller systems for small electric aircraft, Dissertation (2016)
3. Ortun, B.: A coupled RANS/lifting-line analysis for modelling the aerodynamics of distributed propulsion. In: Conference Paper, AHS Technical Conference on Aeromechanics (2018)
4. Veldhuis, L.L.M.: Propeller wing aerodynamic interference. Delft University of Technology: Dissertation (2005)
5. Draper, J., Kuhn, R.: Investigation of the aerodynamic characteristics of a model wing-propeller combination and of the wing and propeller separately at angles of attack up to 90°. Technical Note 3304, NACA (1954)
6. Kuhn, R., Draper, J.: An investigation of a wing-propeller configuration employing large chord plain flaps and large diameter propellers for low speed flight and vertical take-off. Technical Note 3307, NACA (1954)

7. Kuhn, R., Draper, J.: Investigation of the aerodynamic characteristics of a model wing-propeller combination and of the wing and propeller separately at angles of attack up to 90°. Report 1263 NACA, Washington (1956)
8. Adkins, C., Liebeck, R.: Design of optimum propellers. J. Propul. Power **10**(5), 676–682 (1994)
9. Katz, J., Plotkin, A.: Low-Speed Aerodynamics. Mc Graw-Hill, New York (1991)
10. McCormick, B.: Aerodynamics of V/STOL Flight. Academic Press, New York (1967)

Check for updates

Unsteady Wake and Tailplane Loads of the Common Research Model in Low Speed Stall

Andreas Waldmann[1(✉)], Robert Konrath[2], Thorsten Lutz[1], and Ewald Krämer[1]

[1] Universität Stuttgart, Pfaffenwaldring 21, 70569 Stuttgart, Germany
waldmann@iag.uni-stuttgart.de
[2] Deutsches Zentrum für Luft- und Raumfahrt, Bunsenstr. 10, 37073 Göttingen, Germany

Abstract. Hybrid RANS/LES simulations of the flow around the NASA Common Research Model aircraft configuration were carried out with the focus on understanding the interaction of the separated wake with the tailplane in the presence of massively separated flow on the main wing. Validation of the CFD data using PIV data obtained for the flow conditions at $\alpha = 16°$, $\alpha = 18°$ and $\alpha = 20°$ was carried out, confirming the generally satisfactory performance of the DDES simulations observed in earlier publications. As a next step, the wake characteristics and tailplane forces were evaluated for three angles of attack in order to investigate the flow dynamics in low speed stall. The separation characteristics were found to vary over the span. The wake size and downwash direction varied significantly with higher values of α. The altered wing downwash influenced the tailplane inflow, with the load fluctuations on the latter being significantly affected by the amount of turbulent kinetic energy present in the wake.

Keywords: Aircraft aerodynamics · Wake flows · Post-stall flight

1 Introduction

Aerodynamics at the edges of the flight envelope of large civil aircraft is characterized by challenging flow conditions with high Reynolds numbers and, oftentimes, separation phenomena. The understanding of such conditions involves complex experimental or numerical investigations that are able to capture or resolve large scale unsteadiness. This motivated works such as Lutz et al. [6] and Waldmann et al. [12] in the context of the European project ESWI^{RP}, which shed light onto the flow physics of civil aircraft at high Reynolds number stall conditions.

Low speed stall describes a condition at subsonic Mach numbers and relatively high angles of attack. The aircraft's angle of attack is significantly above $\alpha(C_{L,max})$, with the lift coefficient C_L typically decreasing due to large-scale flow separation. Such high angles of attack are encountered on a regular basis by

© Springer Nature Switzerland AG 2020
A. Dillmann et al. (Eds.): DGLR 2018, NNFM 142, pp. 14–24, 2020.
https://doi.org/10.1007/978-3-030-25253-3_2